CrossMark

ORIGINAL PAPER

Static and dynamic magnetic properties of two synthetic francisites Cu$_3$La(SeO$_3$)$_2$O$_2$X (X = Br and Cl)

M. M. Markina[1] · K. V. Zakharov[1] · E. A. Zvereva[1] · R. S. Denisov[1] ·
P. S. Berdonosov[1] · V. A. Dolgikh[1] · E. S. Kuznetsova[1] · A. V. Olenev[1,2] · A. N. Vasiliev[1,3]

Abstract The formation of long-range magnetic order at low temperatures was established in francisite—type compounds Cu$_3$La(SeO$_3$)$_2$O$_2$X (X = Br and Cl) through measurements of magnetic susceptibility, magnetization, specific heat and X-band electron spin resonance. The significantly enhanced critical index $p = 1.0 \pm 0.1$ in Cu$_3$La(SeO$_3$)$_2$Br and $p = 0.8 \pm 0.1$ in Cu$_3$La(SeO$_3$)$_2$Cl in the temperature dependence of the width of ESR signal evidence the reduced dimensionality of the kagome-type francisite's magnetic subsystem. Under action of external magnetic field, the presumably non-collinear six-sublattices antiferromagnetic structure of these compounds experiences the first-order metamagnetic transformation. The B–T magnetic phase diagrams were established from the positions of singularities in temperature and field dependences of thermodynamic properties. Contrary to pristine mineral Cu$_3$Bi(SeO$_3$)$_2$Cl, no signature of structural phase transition was detected.

Keywords Francisite · Metamagnetism · Magnetic phase diagram · Electron spin resonance

Introduction

The compounds belonging to the family of francisite, Cu$_3$Bi(SeO$_3$)$_2$O$_2$Cl, are in the focus of intensive research due to peculiar features of their crystal (Pring et al. 1990; Nazarchuk et al. 2000) and magnetic (Pregelj et al. 2012) structures. In the row of minerals with reduced dimensionality of magnetic subsystem, francisite stands for unique combination of chemical elements, some of them being susceptible for isovalent substitutions. The magnetism in francisite is due to the copper ions Cu^{2+} (3d^9, S = ½), which constitute the kagome-type lattice (Millet et al. 2001; Miller et al. 2012).

In variance with thoroughly studied herbertsmithite, ZnCu$_3$(OH)$_6$Cl$_2$, where kagome network is coupled by antiferromagnetic exchange interactions (Olariu et al. 2008), the francisite is characterized by fierce competition of ferromagnetic and antiferromagnetic exchange (Zakharov et al. 2014; Rousochatzakis et al. 2015). Resulting from this competition is quite unusual six-sublattices non-collinear magnetic structure established in neutron scattering experiment (Pregelj et al. 2012). As follows from the first principles calculations, an antisymmetric Dzyaloshiski–Moriya interaction is important to form such a structure (Rousochatzakis et al. 2015).

At present, unclear is the role of various factors influencing the behavior of francisites. Thus, the structural phase transition in mineral francisite, Cu$_3$Bi(SeO$_3$)$_2$O$_2$Cl, is absent in its synthetic counterpart, Cu$_3$Bi(SeO$_3$)$_2$O$_2$Br (Gnezdilov et al. 2016). The temperature of long-range antiferromagnetic transition changes non-monotonously depending on the size of rare-earth ions. Of significant interest are the mechanisms of magnetic interactions of transition metal and rare-earth subsystems in these objects (Zakharov et al. 2016a, b). This work is devoted to compounds with non-magnetic rare earth, Cu$_3$La(SeO$_3$)$_2$O$_2$X (X = Br and Cl), which should constitute the background for the forthcoming research.

✉ A. N. Vasiliev
anvas2000@yahoo.com

1   M.V. Lomonosov Moscow State University, Moscow, Russia 119991

2   SineTheta Ltd., Moscow, Russia 119992

3   Ural Federal University, Ekaterinburg, Russia 620002

Synthesis and characterization

The crystal structure of mineral $Cu_3Bi(SeO_3)_2O_2Cl$ is shown in Fig. 1. The Bi^{3+} ions are eight-coordinated by oxygen ions O^{2-} forming LaO_8 polyhedron. The unit cell contains Cu^{2+} ions in two distinct positions, Cu1 and Cu2, both in square oxygen environment CuO_4. The squares sharing the common vertices constitute buckled planes with magnetic ions arrangement corresponding to kagome lattice. The Se^{4+} ions coordinated by three oxygen ions form SeO_3 pyramids. One O^{2-} ion of SeO_3 group belongs to Cu_2O_4 square, while two other O^{2-} ions of SeO_3 group belong to two $Cu1O_4$ squares. The Cl^- ions are situated in the tunnels of crystal structure, their mobility being restricted by Se^{4+} lonely electronic pairs (Oliver 2009).

$Cu_3La(SeO_3)_2O_2X$ compounds (X = Br and Cl) were prepared from a stoichiometric mixture of high-purity La_2O_3, CuO, anhydrous $CuBr_2$ or $CuCl_2$, and SeO_2. The selenium dioxide was obtained from selenous acid (99+), which was dehydrated under dynamic vacuum at a moderate temperature and then sublimed in a flowing mixture of dry air and NO_2 prepared by thermal decomposition of $Pb(NO_3)_2$. All preparatory procedures with SeO_2 were carried out in a dry box purged with argon. Lanthanum oxide was additionally calcined in alumina crucible at 1100 °C for 48 h before using. The reactant mixture was thoroughly ground in an agate mortar in argon atmosphere and transferred into quartz tube which was sealed under vacuum about 40–50 mTorr and placed into an annealing furnace with controlled heating. The mixture was heated to 300 °C over 12 h and kept at this temperature for 24 h. Then, the temperature was raised to 575 °C over 12 h and maintained at this temperature for 72 h. After that, furnace was switched off and cooled down to the room temperature. This produced green-colored powder products.
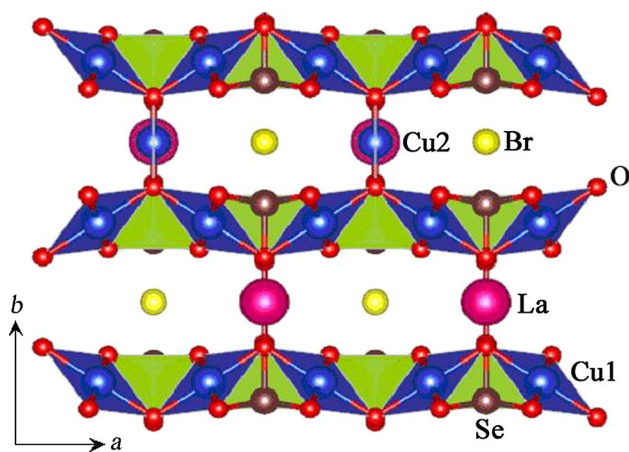
The characterization of samples was performed on STOE STADI P diffractometer (germanium monochromator, $CuK\alpha_1$ radiation, 2θ range 10°–85°, equipped with IP-PSD detector) with ICDD PDF-2 database as reference. The PXRD patterns were indexed in orthorhombic cells in space group $Pmmn$ with cell constants $a = 6.394(2)$ Å, $b = 9.738(3)$ Å, $c = 7.157(3)$ Å, cell volume 445.7(4) Å^3 [Figure of Merit $F(30) = 22.9$] for $Cu_3La(SeO_3)_2O_2Cl$ and $a = 6.4054(23)$ Å, $b = 9.764(3)$ Å, $c = 7.1862(21)$ Å and cell volume 449.4(3) Å^3 [Figure of Merit $F(30) = 22.9$] for $Cu_3La(SeO_3)_2O_2Br$. These data are in good agreement with previously reported for $Cu_3La(SeO_3)_2O_2X$ (Berdonosov and Dolgikh 2008) confirming the obtaining of target compound isostructural to pristine francisite.

Structure refinement for $Cu_3La(SeO_3)_2O_2X$ was performed by Rietveld method on powder samples using STOE Theta/Theta and STOE STADI P diffractometers and JANA 2006 software (Petricek et al. 2014). The final refinement parameters and experimental data are summarized in Table 1. It should be noted that X-ray pattern from bromide compound indicates presence of $La_2Cu(SeO_3)_4$ (Harrison and Zhang 1997). The amount of $La_2Cu(SeO_3)_4$ was estimated as 2.48% in mass. The final Rietveld plots for $Cu_3La(SeO_3)_2O_2X$ compounds are presented in Fig. 2. The atomic coordinates and atomic displacement parameters are listed in Table 2. Interatomic distances are shown in Table 3.

Fig. 1 Crystal structure of mineral $Cu_3Bi(SeO_3)_2O_2Cl$

Table 1 Rietveld refinement data for $Cu_3La(SeO_3)_2O_2X$ (X = Br and Cl) compounds

Composition	$Cu_3La(SeO_3)_2O_2Cl$	$Cu_3La(SeO_3)_2O_2Br$
Symmetry	Orthorhombic	
Space group	$Pmmn$	
Cell constants		
a (Å)	6.39407 (18)	6.40071 (5)
b (Å)	9.7310 (3)	9.75675 (7)
c (Å)	7.1547 (2)	7.17800 (5)
V (Å^3)	445.17 (2)	448.267 (6)
Z	2	
Density calc (g/cm^3)	4.8559	5.1517
Instrument	STOE theta/theta	STOE STADI P
Temperature	293	
Wavelength (Å)	1.5418	1.5406
Software	JANA2006	
Absorption coefficient (μ mm^{-1})	56.779	59.611
2θ range (°)	10–100	5–110
R	0.0370	0.0227
wR	0.0345	0.0278
Goodness of fit	1.32	1.67

(a)

(b)
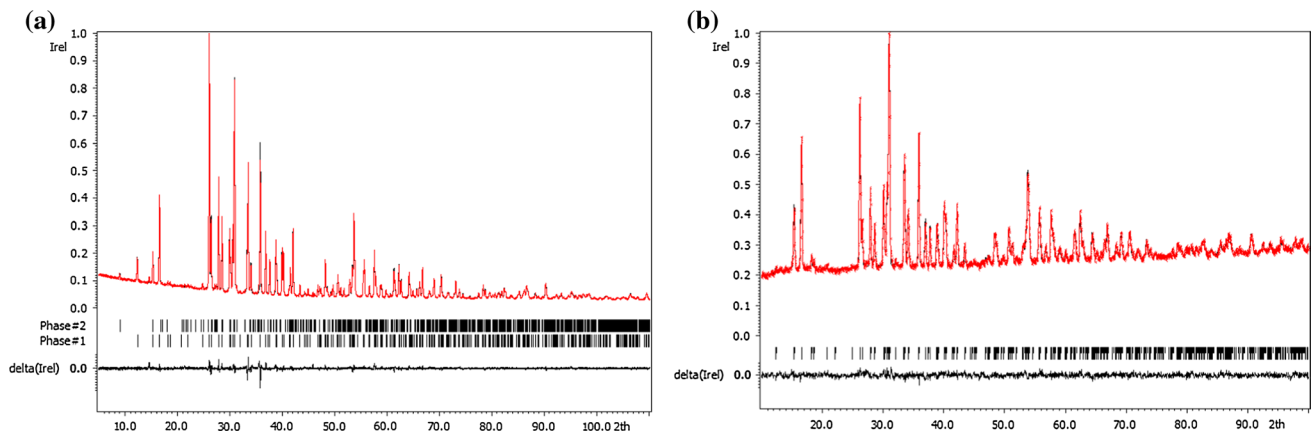
Fig. 2 Rietveld plots for $Cu_3La(SeO_3)_2O_2Br$ (**a**) and $Cu_3La(SeO_3)_2O_2Br$ (**b**) structure refinements

Table 2 Atomic coordinates and isotropic thermal parameters (Å^2) for $Cu_3La(SeO_3)_2O_2X$ (X = Br and Cl) crystal structures

Atom	Wyck	x	y	z	U
$Cu_3La(SeO_3)_2O_2Cl$					
La_1	2a	1/4	1/4	0.2676 (4)	0.0124 (10)
Cu_1	4c	0	0	0	0.0273 (16)
Cu_2	2a	1/4	1/4	0.8000 (9)	0.022 (2)
Se_1	4e	1/4	0.5517 (4)	0.6018 (5)	0.0193 (13)
O_1	4e	1/4	0.1088 (16)	0.995 (2)	0.021 (6)
O_2	8g	0.0339 (16)	0.5827 (11)	0.7406 (19)	0.020 (4)
O_3	4e	1/4	0.1208 (16)	0.582 (2)	0.010 (6)
Cl_1	2b	1/4	3/4	0.1391 (15)	0.049 (5)
$Cu_3La(SeO_3)_2O_2Br$					
La_1	2a	1/4	1/4	0.26648 (10)	0.0059 (2)
Cu_1	4c	0	0	0	0.0172 (4)
Cu_2	2a	1/4	1/4	0.7998 (2)	0.0108 (5)
Se_1	4e	1/4	0.55164 (10)	0.60166 (12)	0.0119 (3)
O_1	4e	1/4	0.1108 (5)	0.9902 (6)	0.0102 (8)
O_2	8g	0.0441 (5)	0.5785 (3)	0.7458 (4)	0.0102 (8)
O_3	4e	1/4	0.1217 (5)	0.5841 (6)	0.0102 (8)
Br_1	2b	1/4	3/4	0.15337 (17)	0.0218 (5)

Table 3 Interatomic distances (Å) for $Cu_3La(SeO_3)_2O_2X$ (X = Br and Cl) crystal structures

$Cu_3La(SeO_3)_2O_2Cl$			$Cu_3La(SeO_3)_2O_2Br$		
Bond		Distance	Bond		Distance
$La_1–O_1$	x2	2.386 (15)	$La_1–O_1$	x2	2.404 (5)
$La_1–O_2$	x2	2.439 (10)	$La_1–O_2$	x2	2.520 (3)
$La_1–O_3$	x2	2.577 (15)	$La_1–O_3$	x2	2.601 (4)
$La_1–O2$	x2	2.439 (10)	$La_1–O_2$	x2	2.520 (3)
$Cu_1–O_1$	x2	1.918 (9)	$Cu_1–O_1$	x2	1.932 (3)
$Cu_1–O_2$	x2	2.034 (13)	$Cu_1–O_2$	x2	1.999 (3)
$Cu_2–O_1$	x2	1.958 (16)	$Cu_2–O_1$	x2	1.927 (5)
$Cu_2–O_3$	x2	2.003 (16	$Cu_2–O_3$	x2	1.991 (5)
$Se_1–O_2$	x2	1.728 (12)	$Se_1–O_2$	x2	1.696 (3)
$Se_1–O_3$		1.685 (16)	$Se_1–O_3$		1.696 (5)

Electron spin resonance

Dynamic magnetic properties were investigated by means of X-band electron spin resonance setup CMS 8400 "Adani" ($f \approx 9.4$ GHz, $B \leq 0.7$ T) in the range 5–300 K. The temperature evolution of the first derivative of ESR absorption dP/dB for the powder samples $Cu_3La(SeO_3)_2O_2Br$ and $Cu_3La(SeO_3)_2O_2Cl$ is shown in Figs. 3a and 4a. In general, both samples demonstrate the similar behavior,

revealing the single ESR signal, which broadens continuously in the wide temperature range. The main difference is a strong lineshape distortion, which is clearly seen below 70 K for the chloride sample (Fig. 4a) reflecting probably the presence of an additional impurity mode in the dynamic response. To determine the main parameters of ESR spectra, the analysis of the line shape was performed by fitting of experimental spectra to the Lorentzian profile and taking into account two circular components of linearly polarized microwave field (Ivanshin et al. 2000)

$$\frac{dP}{dB} \propto \frac{d}{dB}\left[\frac{\Delta B}{(B - B_r)^2 + \Delta B^2} + \frac{\Delta B}{(B + B_r)^2 + \Delta B^2}\right], \quad (1)$$

where B_r is the resonance field and ΔB is the width of the absorption line. To account for the line distortion in the chloride sample, we have also included another component in the form of Eq. (1) to separate and analyze the parameters of main mode. The temperature dependence of the main ESR parameters (namely, the effective g-factor,
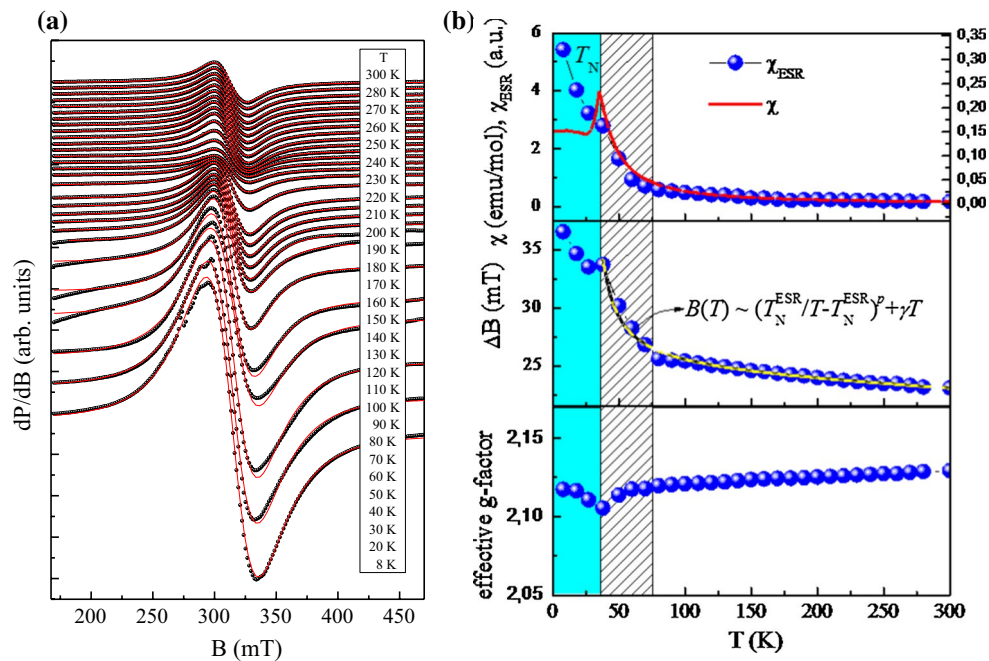
Fig. 3 a Temperature evolution of ESR spectra in $Cu_3La(SeO_3)_2O_2Br$. The experimental data are represented by *symbols*, the fitting curves are shown by *solid lines*. **b** Temperature dependences of effective *g*-factor (*lower panel*), width of line (*middle panel*) and integral intensity of ESR signal (*upper panel*) in $Cu_3La(SeO_3)_2O_2Br$

the ESR linewidth and the integral ESR intensity) is collected in Figs. 3b and 4b. In the paramagnetic phase, the absorption is characterized by an almost temperature-independent effective *g*-factor, which takes value as about $g = 2.13 \pm 0.03$ and $g = 2.14 \pm 0.03$ for bromide and chloride samples, respectively, in a good correspondence with those found for other francisites (Wang et al. 2012;

Zakharov et al. 2014, 2016a, b). Below ~70 K for bromide and ~40 K for chloride samples, respectively, the effective *g*-factor deviates from its constant value indicating the appearance of short-range correlations and fluctuating internal fields upon approaching the magnetic phase transition. At the same time, the ESR linewidth of both samples increases at cooling over whole temperature range. Both

Fig. 4 a Temperature evolution of ESR spectra in $Cu_3La(SeO_3)_2O_2Cl$. The experimental data are represented by *symbols*, the fitting curves are shown by *solid lines*. **b** Temperature dependences of effective *g*-factor (*lower panel*), width of line (*middle panel*) and integral intensity of ESR signal (*upper panel*) in $Cu_3La(SeO_3)_2O_2Cl$
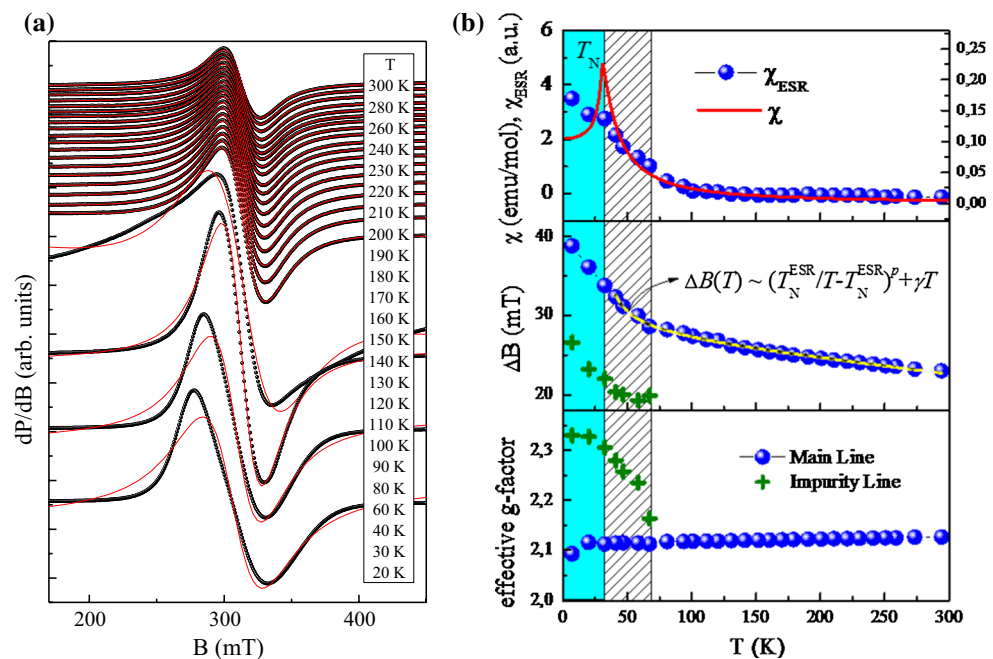
g-factor and ΔB exhibit clear anomalies at the Neel temperatures confirmed in the magnetic susceptibility and specific heat measurements. The integral ESR intensity, which is proportional to the number of spins for isolating materials, was estimated by double integration of the experimental ESR spectra. Upper panels of Figs. 3b and 4b demonstrate Curie–Weiss behavior with temperature decreasing in satisfactory agreement with magnetic susceptibility data $\chi(T)$ in the paramagnetic phase at $T > T_N$. It should be noted that similarly to the case of $Cu_3Y(SeO_3)_2O_2Cl$ (Zakharov et al. 2014), the absorption line does not disappear below T_N indicating vanishingly small internal magnetic field on copper ions in magnetically ordered state.

The behavior of the ESR linewidth for investigated samples reveals three distinctly different spin dynamic regimes in the temperature range studied. It increases weakly and almost linearly down to 70–80 K. Then, the absorption line exhibits the rapid power-type broadening upon approaching the Neel temperature from above. Eventually, after passing through an anomaly in the proximity of the T_N, the linewidth once again shows an additional increase at $T < T_N$, which perhaps indicates non-saturation of the spin-correlations length even in ordered state similarly to other members of this family (Zakharov et al. 2014). Such a broadening of ESR line is associated usually with a slowing down of the spin fluctuations in the vicinity of the critical temperature. This causes the divergence of spin-correlation length, which, in turn, affects the spin–spin relaxation time of the exchange-narrowed ESR line. Consequently, these processes should lead to the critical behavior in vicinity of Neel temperature and also to be dependent on the dimensionality of the magnetic subsystem. In the frames of this model (Mori and Kawasaki 1962; Kawasaki 1968a, b; Huber 1972), the temperature dependence of ΔB can be described by the following formula

$$\Delta B(T) = \Delta B^* + A \cdot \left[\frac{T_N^{ESR}}{T - T_N^{ESR}} \right]^p, \tag{2}$$

where the first term ΔB^* describes the high-temperature limit of the exchange-narrowed resonance line and second term is responsible for the critical behavior upon approaching the order–disorder temperature T_N^{ESR} from above, p is the critical index. Taking into account the linear increase in the ESR linewidth width at elevated temperatures, we modified this equation by adding an additional linear term γT following the earlier suggested procedure (Zvereva et al. 2015). The solid black curves in the middle panels of Figs. 3b and 4b represent the result of these approximations. The best agreement for the $Cu_3La(SeO_3)_2O_2Br$ sample was obtained at $A = 5 \pm 1$ mT, $\Delta B^* = 25 \pm 1$ mT, $T_N^{ESR} = 27 \pm 5$ K, $\gamma = -0.006$ mT/K and $p = 1.0 \pm 0.1$. The corresponding values for $Cu_3La(SeO_3)_2O_2Cl$ sample

are $A = 3 \pm 1$ mT, $\Delta B^* = 27 \pm 1$ mT, $T_N^{ESR} = 30 \pm 5$ K, $\gamma = -0.002$ mT/K and $p = 0.8 \pm 0.1$. Note that in the frame of Kawasaki's approach, the critical index of ESR linewidth can be written as

$$p = \frac{7 + \eta}{2\nu} - 2(1 - \alpha), \tag{3}$$

where ν describes the divergence of correlation length, η is the critical parameter of the divergence of static correlations, and α relates to the specific heat divergence. Assuming $\eta = \alpha = 0$ and $\nu = 2/3$ for three-dimensional antiferromagnet (Kawasaki 1968a, b), the value of p should be equal to 1/3 which is significantly lower than the estimated values for both compounds. So, our ESR date indicate the reduced dimensionality of the magnetic interactions for both new members of the francisite family.

Thermodynamic properties

The physical properties of new compounds were characterized in measurements of magnetic susceptibility χ, magnetization M, specific heat C_p using commercial Physical Properties Measurements System "Quantum Design" PPMS-9T in the temperature range 2–300 K up to $B = 9$ T. The temperature dependences of magnetic susceptibility χ in $Cu_3La(SeO_3)_2O_2X$ (X = Br and Cl) taken at $B = 1$ T are shown in Fig. 5a, b. In the range 200–300 K, these dependences follow the Curie–Weiss law with inclusion of temperature-independent term

$$\chi = \chi_0 + \frac{C}{T - \Theta} \tag{4}$$

with parameters presented in Table 4. The positive value of Weiss temperature Θ indicates domination of ferromagnetic exchange interaction at elevated temperatures in both compounds. The values of Curie constant C allows estimation of the square of effective magnetic moment per Cu^{2+} ion which corresponds to *g*-factor in good agreement with ESR measurements. The temperature-independent term is due to summation of diamagnetic Pascal's constants of individual ions (Bain and Berry 2008) and paramagnetic van Vleck contribution of Cu^{2+} ions (Banks et al. 2009) constituting $\chi_0 = -(5.0 \pm 0.3) \times 10^{-4}$ emu/mol in both compounds. The fitting curves are shown by dashed lines in Fig. 5a, b. The right axis of this figure represents the temperature dependence of Curie constant C. At cooling below ~150 K, the $\chi(T)$ dependences deviate from Curie–Weiss law and exhibit sharp singularities at Neel temperatures. Similar behavior was seen earlier in $Cu_3Y(SeO_3)_2O_2Cl$ (Zakharov et al. 2014) where neutron scattering measurements established formation of six-sublattices non-collinear structure due to fierce competition of
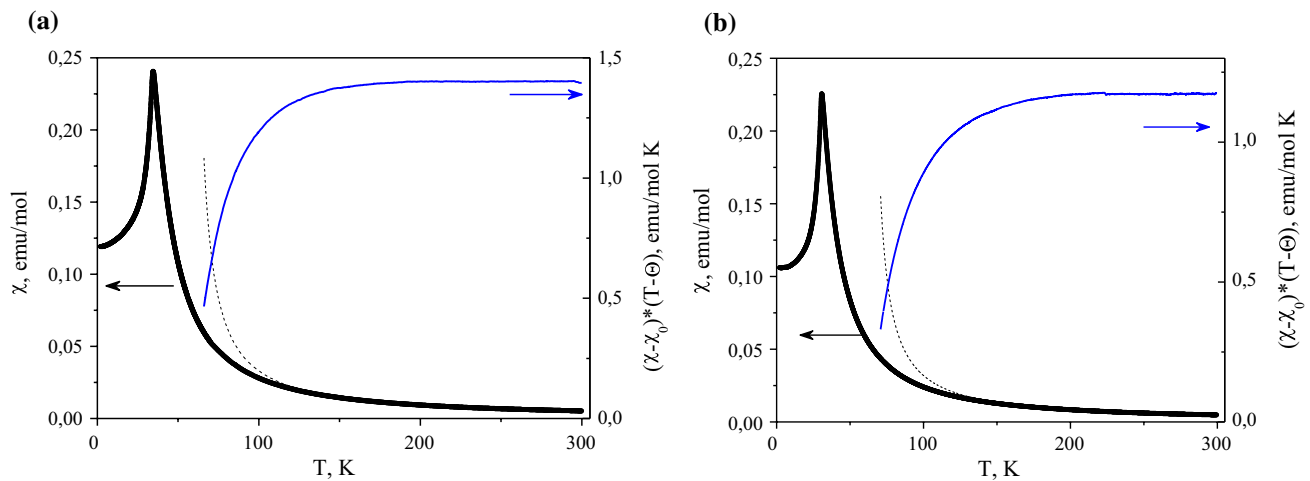
(a)

(b)

Fig. 5 Temperature dependence of magnetic susceptibility taken at $B = 1$ T. The *dashed line* represents the fitting according to the Curie–Weiss law. *Solid line* shows the temperature dependence of the Curie constant (*right axis*) in $Cu_3La(SeO_3)_2O_2Br$ (**a**) and $Cu_3La(SeO_3)_2O_2Cl$ (**b**)

Table 4 Magnetic subsystem parameters in $Cu_3La(SeO_3)_2O_2X$ (X = Br and Cl)

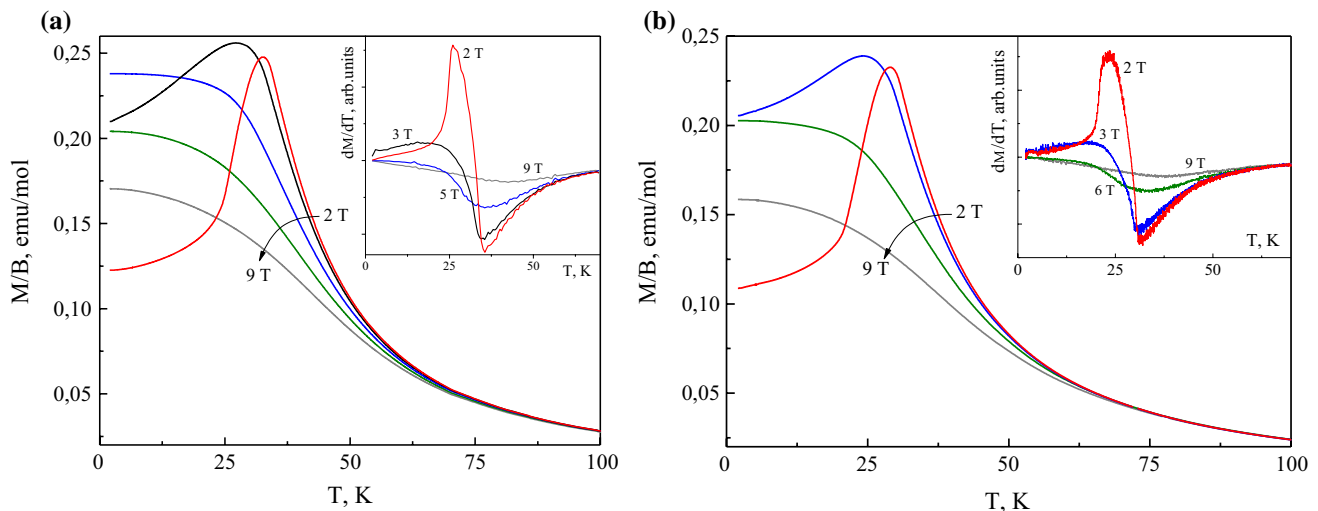| Compound	T_N (K)	C (emu/mol K)	θ (K)	μ_{eff}^2 (μ_B)	g	B_C (T) (at 5 K)
$Cu_3La(SeO_3)_2O_2Br$	34.3	1.43	55.1	11.4	2.13	2.45
$Cu_3La(SeO_3)_2O_2Cl$	31.2	1.35	52.9	10.8	2.14	2.40

(a)

(b)

Fig. 6 Temperature dependences of reduced magnetic moment at $B \leq 9$ T in $Cu_3La(SeO_3)_2O_2Br$ (**a**) and $Cu_3La(SeO_3)_2O_2Cl$ (**b**). The *insets* represent the temperature dependences of the derivative dM/dT

antiferromagnetic and ferromagnetic exchange interactions. The temperature dependences of reduced magnetic moment M/B taken at several values of magnetic field up to 9 T are shown in Fig. 6a, b. Under magnetic field, the anomalies at T_N smear and shift to lower temperatures. The insets to Fig. 6a, b represent the derivatives of magnetization dM/dT

which underline qualitative change taking place between 2 and 3 T which is further supported by $M(B)$ measurements.

The field dependences of magnetization $M(B)$ taken at various temperatures in the range 2–35 K are shown in Fig. 7a, b. The linear dependence $M(B)$ seen at low magnetic field is followed by sharp increase at critical field
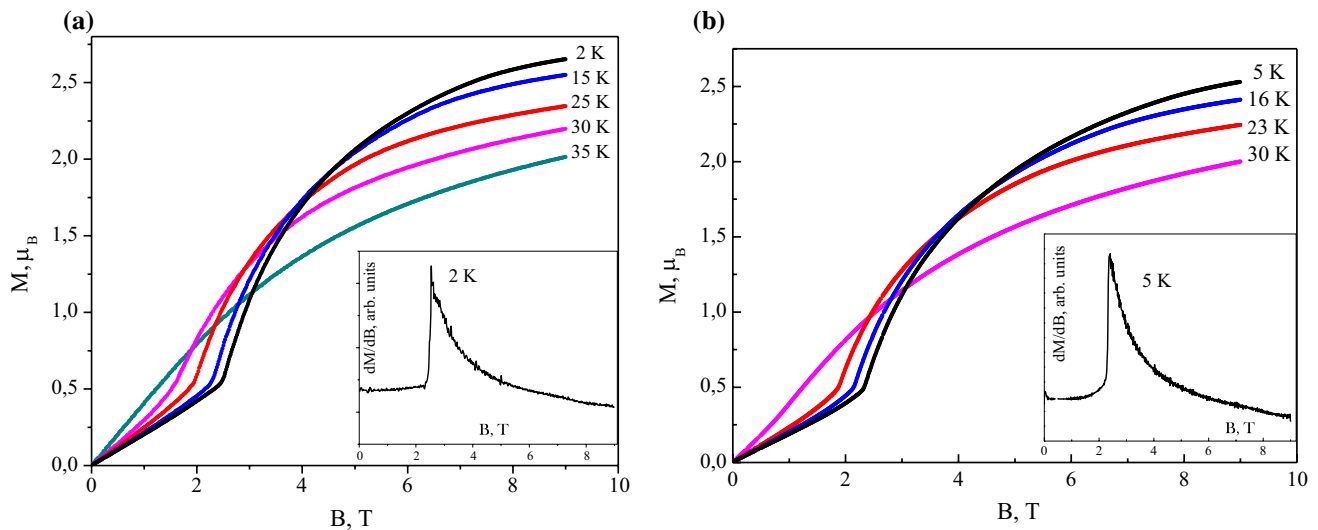
Fig. 7 Field dependences of magnetization in $Cu_3La(SeO_3)_2O_2Br$ (**a**) and $Cu_3La(SeO_3)_2O_2Cl$ (**b**) at $T \leq 35$ K. The *insets* represent the field dependence of derivative dM/dB

B_C and tendency to saturation at high magnetic field. We believe that a metamagnetic transition takes place at B_C in $Cu_3La(SeO_3)_2O_2Br$ (X = Br and Cl) when antiferromagnetic ordering along c axis is destroyed by external field but non-collinear ferrimagnetic FM structure is preserved in *ab* plane. At $B > B_C$, the gradual alignment of Cu^{2+} magnetic moments with external magnetic field occurs. In the range of magnetic field studied, the magnetization reaches $M \sim 2.5 \mu_B$ per formula unit at 2 K which is lower than expected saturation $M_S = 3g S\mu_B \sim 3.2 \mu_B$. The insets to Fig. 7a, b represent the derivatives dM/dB at 2 K which clearly emphasize anomalies at $B_C \sim 2.5$ T. At higher temperatures, the anomalies in $M(B)$ and dM/dB curves shift to lower magnetic field and disappear at $T \sim T_N$ which corresponds to transition of $Cu_3La(SeO_3)_2O_2X$ (X = Br and Cl) into paramagnetic state.

The temperature dependences of specific heat $C_p(T)$ in the range 2–50 K at several values of magnetic field up to 9 T are shown in Fig. 8a, b. At $T \sim T_N$, the $C_p(T, B = 0)$ curves demonstrate sharp λ-type anomalies accompanying transition between antiferromagnetic AFM and paramagnetic PM phases. Under external magnetic field, the anomalies smear and shift to lower temperatures. The low-temperature specific heat in the range 2–12 K was fitted by the sum

$$C_p = A_0 T^{3/2} + \beta T^3, \tag{5}$$

where first term represents the contribution of ferromagnetic magnons and the second term is responsible for phonons contribution. The order–disorder transition in magnetic subsystem is accompanied by the release of entropy

$$\Delta S_{mag} = nR \ln(2S + 1), \tag{6}$$

where $n = 3$ is the number of magnetic ions per formula unit, $R = 8.314$ J/mol K is the universal gas constant and $S = ½$ is the spin-only magnetic moment of copper ions. For any francisite with non-magnetic rare earth, the expected value of magnetic entropy is 17.3 J/mol K. To estimate roughly the magnetic entropy released at phase transition in $Cu_3La(SeO_3)_2O_2Br$, one has calculate the area under $(C_p(T, 9 \text{ T}) - C_p(T, 0 \text{ T}))/T$ curve. This procedure gives $\Delta S_{mag} \sim (4.5 \pm 0.25)$ J/mol K for both compounds which constitute only small portion of total magnetic entropy. This means that the significant part of magnetic entropy is released at much higher temperatures in full correspondence with deviation of magnetic susceptibility χ from the Curie–Weiss law at $T < 150$ K. The behavior of this type is typical for low-dimensional magnetic systems where short-range magnetic correlations develop far above the Neel temperature.

The study of thermodynamic properties of $Cu_3La(SeO_3)_2O_2X$ (X = Br and Cl) resulted in magnetic phase diagrams shown in the insets to Fig. 8a, b. Three regions can be separated in these diagrams corresponding to paramagnetic PM phase, antiferromagnetic AFM phase and ferrimagnetic FM phase. The PM boundary was defined by λ-type anomalies at $C_p(T)$ curves and peaks at $\chi(T)$ curves. The AFM–FM boundary was defined by peaks at $dM/dB(T)$ curves. This boundary is shown by dashed line since its position depends on sign of dB/dT variation as assumed for the first-order metamagnetic transition.
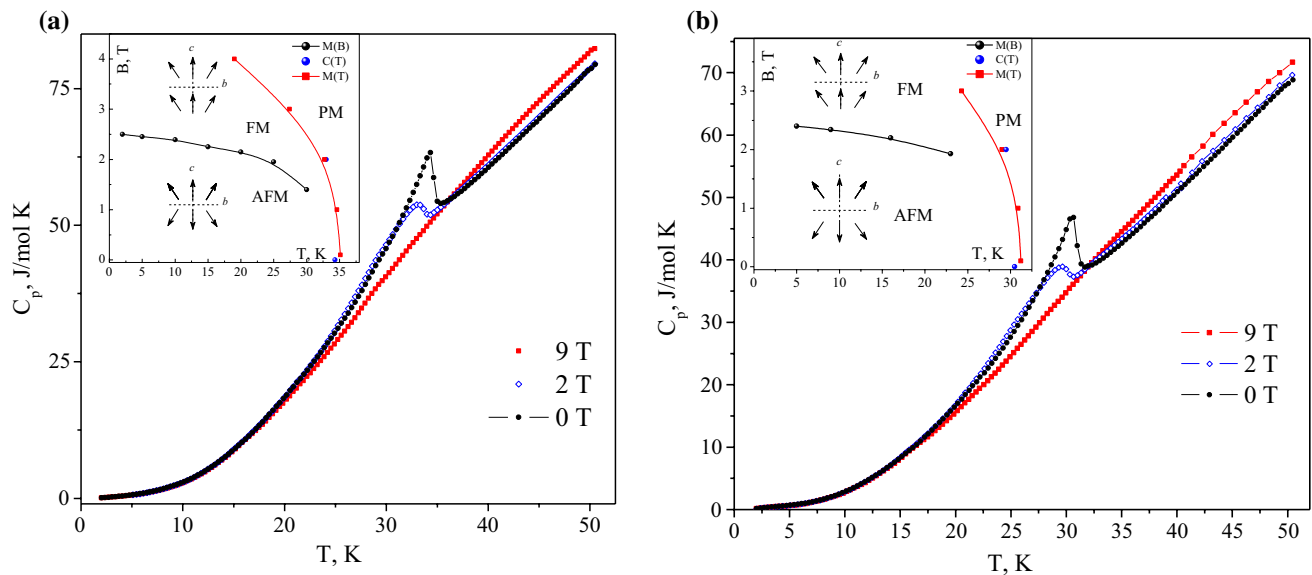
(a)

(b)

Fig. 8 Temperature dependences of specific heat in $Cu_3La(SeO_3)_2O_2Br$ (**a**) and $Cu_3La(SeO_3)_2O_2Cl$ (**b**) at several magnetic fields $B \leq 9$ T. The *insets* represent the phase diagram of the title compounds. The *arrows* indicate directions of individual magnetic moments of Cu^{2+} ions in AFM and FM phases

Conclusion

Study of static and dynamic magnetic properties of $Cu_3La(SeO_3)_2O_2X$ (X = Br and Cl) established formation of the long-range magnetic order at low temperatures. These temperatures are marked by λ-type anomaly in specific heat. The positive value of Weiss temperature evidences the predominance of ferromagnetic interactions at elevated temperatures. The deviation of magnetic susceptibility from the Curie–Weiss law at lowering temperature reveals significant short-range antiferromagnetic correlations below 150 K. This fact is in correspondence with reduced dimensionality of magnetic subsystem as found in ESR measurements. The metamagnetic phase transition found in both compounds at $T < T_N$ is of practical significance since it is associated with broadband absorption of electromagnetic radiation that spans over several decades in frequency. This property is highly praised in modern electronics (Zorko et al. 2016). No signature of structural phase transition present in pristine mineral, $Cu_3Bi(SeO_3)_2O_2Cl$ was detected signaling important role Bi^{3+} ions lonely pair.

References

Bain GA, Berry JF (2008) Diamagnetic corrections and Pascal's constants. J Chem Educ 85:532

Banks MG, Kremer RK, Hoch C, Simon A, Ouladdiaf B, Broto JM, Rakoto H, Lee C, Whangbo MH (2009) Magnetic ordering in the frustrated Heisenberg chain system cupric chloride $CuCl_2$. Phys Rev B 80:024404

Berdonosov PS, Dolgikh VA (2008) Copper lanthanide selenite oxohalides with francisite structure: synthesis and structural characteristics. Russ J Inorg Chem 53:1353

Gnezdilov V, Pashkevich Y, Kurnosov V, Lemmens P, Kuznetsova E, Berdonosov P, Dolgikh V, Zakharov K, Vasiliev A (2016) Longitudinal magnon, inversion breaking and magnetic instabilities in the pseudo-Kagome francisites $Cu_3Bi(SeO_3)_2O_2X$ with X = Br, Cl. arXiv:1604.04249

Harrison WTA, Zhang Zh (1997) Synthesis and Crystal Structure of $La_2Cu(SeO_3)_4$. J Solid State Chem 133:572

Huber DL (1972) Critical-point anomalies in the electron-paramagnetic-resonance linewidth and in the zero-field relaxation time of antiferromagnets. Phys Rev B 6:3180

Ivanshin VA, Deisenhofer J, Krug von Nidda HA, Loidl A, Mukhin A, Balbashov J (2000) ESR study in lightly doped $La_{1-x}Sr_xMnO_3$. Phys Rev B 61:6213

Kawasaki K (1968a) Anomalous spin relaxation near the magnetic transition. Prog Theor Phys 39:285

Kawasaki K (1968b) Ultrasonic attenuation and ESR linewidth near magnetic critical points. Phys Lett A 26:543

Miller KH, Stephens PW, Martin C, Constable E, Lewis RA, Berger H, Carr GL, Tanner DB (2012) Infrared phonon anomaly and magnetic excitations in single-crystal $Cu_3Bi(SeO_3)_2O_2Cl$. Phys Rev B 86:174104

Millet P, Bastide B, Pashchenko V, Gnatchenko S, Gapon V, Ksari Y, Stepanov A (2001) Syntheses, crystal structures and magnetic

properties of francisite compounds $Cu_3Bi(SeO_3)_2O_2X$ (X = Cl, Br and I). J Mater Chem 11:1152

Mori H, Kawasaki K (1962) Antiferromagnetic resonance absorption. Prog Theor Phys 28:971

Nazarchuk EV, Krivovichev SV, Pankratova OY, Filatov SK (2000) Thermal expansion of francisite, $[Cu_3BiO_2](SeO_3)_2Cl$, and its interpretation based on oxocentered copper-bismuth tetrahedral. Phys Chem Miner 27:440

Olariu A, Mendels P, Bert F, Duc F, Trombe JC, de Vries MA, Harrison A (2008) O^{17} NMR Study of the intrinsic magnetic susceptibility and spin dynamics of the quantum kagome Antiferromag netZnCu$_3$(OH)$_6$Cl$_2$. Phys Rev Lett 100:087202

Oliver SRJ (2009) Cationic inorganic materials for anionic pollutant trapping and catalysis. Chem Soc Rev 38:1868

Petricek V, Dusek M, Palatinus L (2014) Crystallographic computing system JANA2006: general features. Z Kristallogr 229:345

Pregelj M, Zaharko O, Günther A, Loidl A, Tsurkan V, Guerrero S (2012) Magnetic ground state and two-dimensional behavior in pseudo-kagome layered system $Cu_3Bi(SeO_3)_2O_2Br$. Phys Rev B 86:144409

Pring A, Gatehouse BM, Birch WD (1990) Francisite, $Cu_3Bi(SeO_3)_2O_2Cl$, a new mineral from Iron Monarch, South Australia; description and crystal structure. Am Miner 75:1421

Rousochatzakis I, Richter J, Zinke R, Tsirlin AA (2015) Frustration and Dzyaloshinsky-Moriya anisotropy in the kagome francisites $Cu_3Bi(SeO_3)_2O_2X$ (X = Br, Cl). Phys Rev B 91:024416

Wang Z, Schmidt M, Goncharov Y, Tsurkan V, Krug von Nidda HA, Loidl A, Deisenhofer J (2012) Terahertz spectroscopy in the pseudo-Kagome system $Cu_3Bi(SeO_3)_2O_2Br$. Phys Rev B 86:174411

Zakharov KV, Zvereva EA, Berdonosov PS, Kuznetsova ES, Dolgikh VA, Clark L, Black C, Lightfoot P, Kockelmann W, Pchelkina ZV, Streltsov SV, Volkova OS, Vasiliev AN (2014) Thermodynamic properties, electron spin resonance, and underlying spin model in $Cu_3Y(SeO_3)_2O_2Cl$. Phys Rev B 90:214417

Zakharov KV, Zvereva EA, Kuznetsova ES, Berdonosov PS, Dolgikh VA, Markina MM, Olenev AV, Shakin AA, Volkova OS, Vasiliev AN (2016a) Two new lanthanide members of francisite family $Cu_3Ln(SeO_3)_2O_2Cl$ (Ln = Eu, Lu). J Alloys Compd 685:442

Zakharov KV, Zvereva EA, Markina MM, Stratan MI, Kuznetsova ES, Dunaev SF, Berdonosov PS, Dolgikh VA, Olenev AV, Klimin SA, Mazaev LS, Kashchenko MA, Ahmed MA, Banerjee A, Bandyopadhyay S, Iqbal A, Rahaman B, Saha-Dasgupta T, Vasiliev AN (2016b) Magnetic, resonance and optical properties of $Cu_3Sm(SeO_3)_2O_2Cl$: a rare earth francisite compound. Phys Rev B 94:054401

Zorko A, Gomilšek M, Pregelj M, Ozerov M, Zvyagin SA, Ozarowski A, Tsurkan V, Loidl A, Zaharko O (2016) Electron spin resonance insight into broadband absorption of the $Cu_3Bi(SeO_3)_2O_2Br$ metamagnet. AIP Adv 6:056210

Zvereva EA, Stratan MI, Ovchenkov YA, Nalbandyan VB, Lin JY, Vavilova EL, Iakovleva MF, Abdel-Hafiez M, Silhanek AV, Chen XJ, Stroppa A, Picozzi S, Jeschke HO, Valentí R, Vasiliev AN (2015) Zigzag antiferromagnetic quantum ground state in monoclinic honeycomb lattice antimonates A3Ni2SbO6(A = Li, Na). Phys Rev B 92:144401